Supporting Information

Ultrahigh Mass-Loading Integrated High Coulombic Efficiency Si-Graphite Electrode for High-Energy-Density Lithium Ion Battery

Shu Zhang[#, a], Yi Zhu[#, a], Xiandi Zhang[a], Fanglin Hu[a], Wengao Zhao[*, b], Jianxuan Du[b], Shuyue Xue[a], Peng Li[*, a] and Yu-Jia Zeng[*, c]

[a] *Department of Chemical Engineering, Shandong University of Technology, 255000, China*

[b] *Institute of Nanotechnology, Karlsruhe Institute of Technology (KIT), 76344 Eggenstein-Leopoldshafen, Germany*

[c] *Key Laboratory of Optoelectronic Devices and Systems of Ministry of Education and Guangdong Province, College of Physics and Optoelectronic Engineering, Shenzhen University, 518060, China*

* *Corresponding author.*

E-mail: Peng.Li.UPC@hotmail.com; wengao.zhao@kit.edu; yjzeng@szu.edu.cn

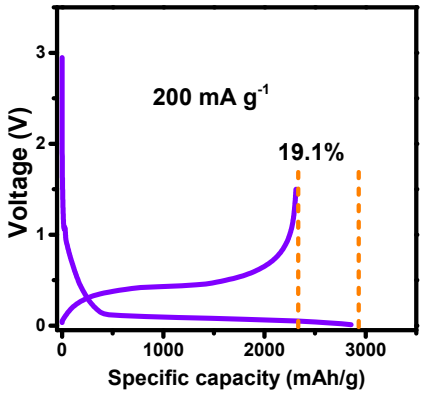

Figure S1. The initial charge/discharge curve of LB-Si/CT

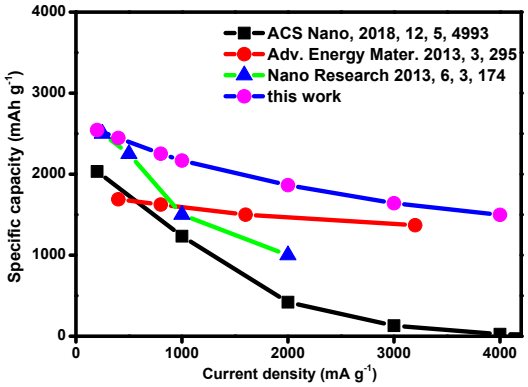

Figure S2. Comparison of rate performance with previous works.

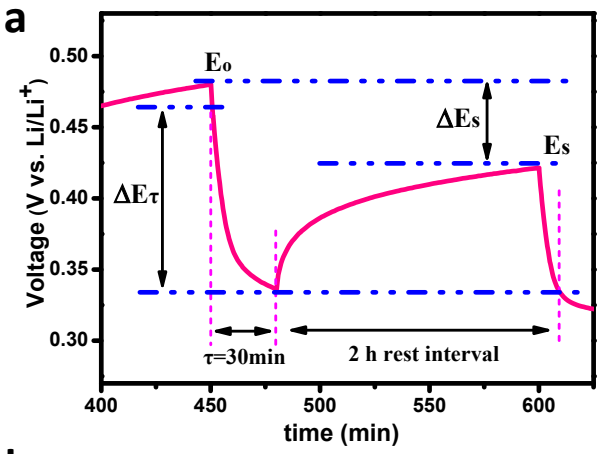

b

$$D = \frac{4}{\pi\tau}\left(\frac{m_B V_M}{M_B S}\right)^2\left(\frac{\Delta E_s}{\Delta E_\tau}\right)^2$$

Figure S3. (a) Schematic representation and (b) simplified equation for diffusion coefficient calculation of the galvanostatic intermittent titration technique (τ: duration of the current pulse; ΔE_S: voltage change due to the current pulse; $\Delta E\tau$: voltage change during the current pulse; m_B, M_B, V_M, and S are the active mass, molar mass, molar volume, and active surface area, respectively).

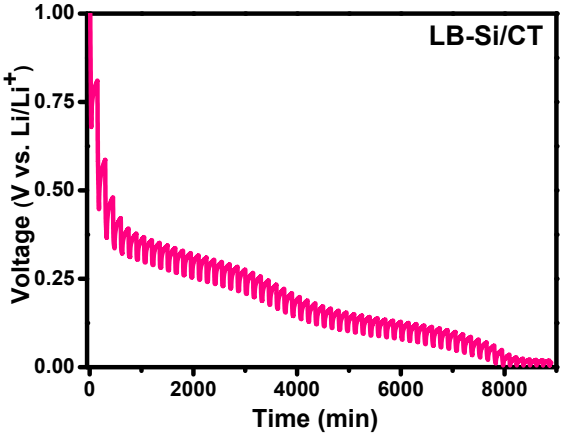

Figure S4. Galvanostatic intermittent titration technique test of LB-Si/CT

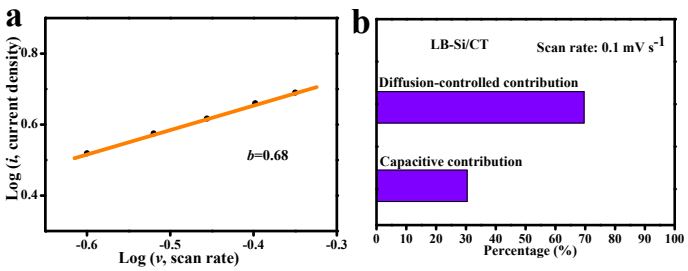

Figure S5. (a) log(i)/log(v) plots of LB-Si/CT at various scan rates from 0.25 to 0.45 mV s^{-1} and (b) contribution ratio of capacitive- and diffusion-controlled charge at 0.1 mV s^{-1}.

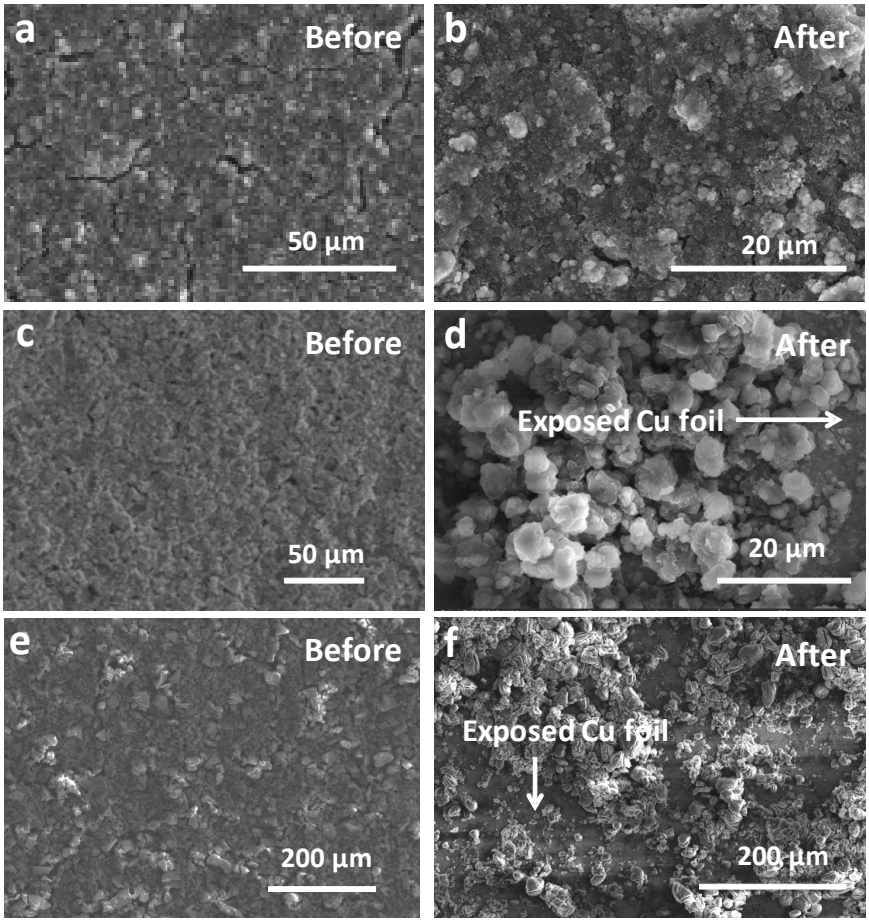

Figure S6. SEM images of (a, b) LB-Si/CT, (c, d) bare Si and (e, f) SiO precursor electrode surface before and after cycling.

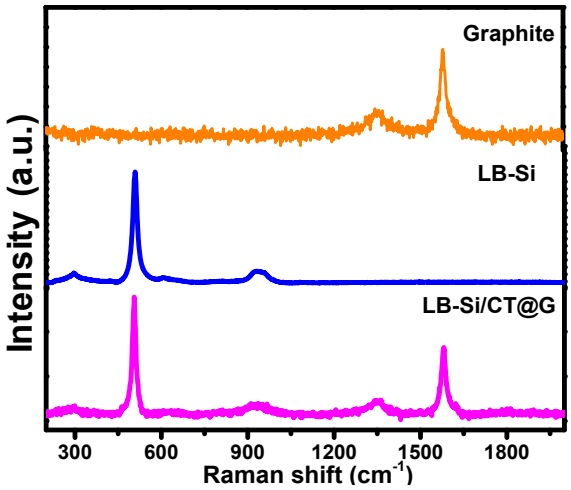

Figure S7. Raman spectra of graphite, LB-Si and LB-Si/CT@G.

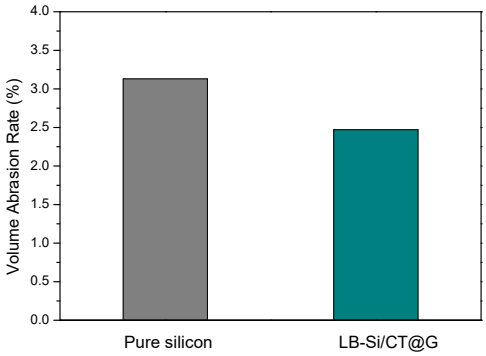

Figure S8. The volume abrasion rate of pure silicon and LB-Si/CT@G electrodes

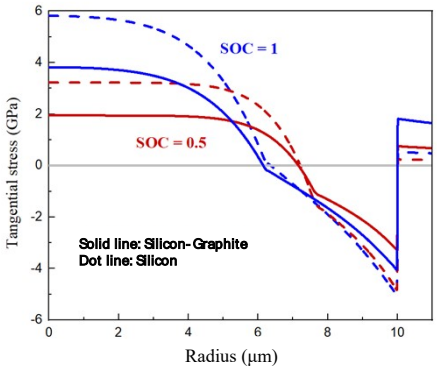

Figure S9. Tangential stress distribution of silicon-graphite electrode at SOC of 0.5 and 1

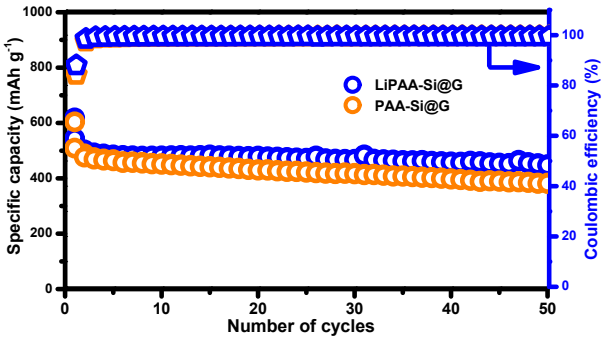

Figure S10. Cycling performance of LB-Si/CT@G electrodes with PAA or LiPAA binder.

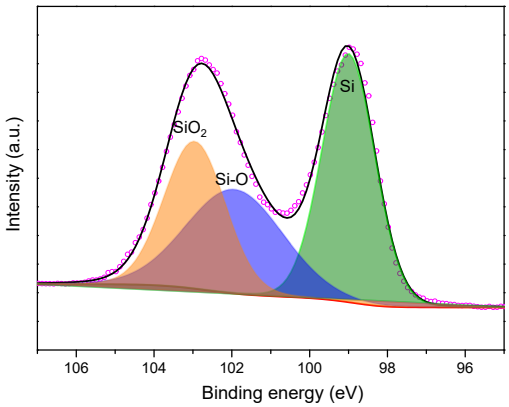

Figure S11. XPS spectra of Si 2p line

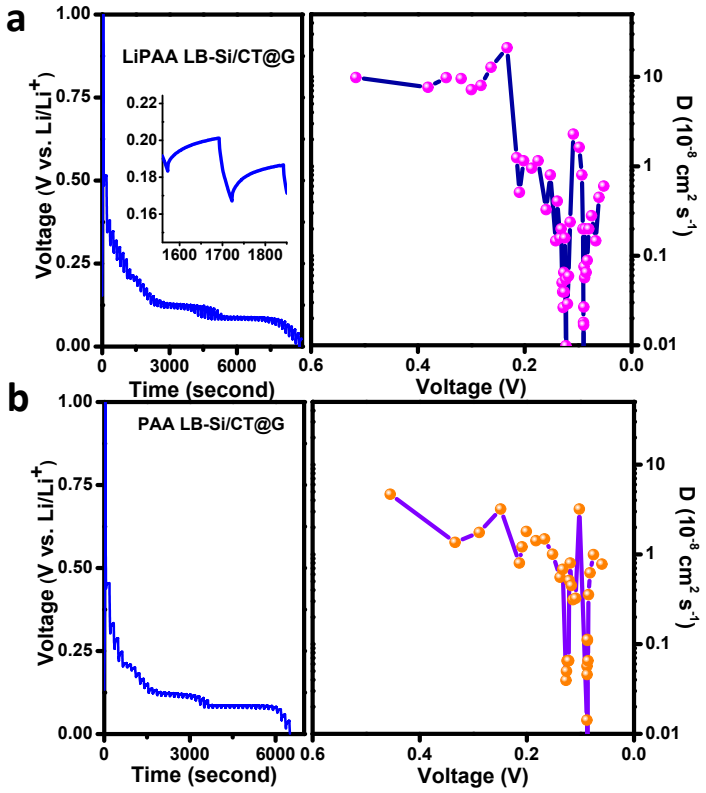

Figure S12. GITT test of LB-Si/CT@G with (a) LiPAA or (b) PAA binder and their corresponding diffusion coefficient plot.

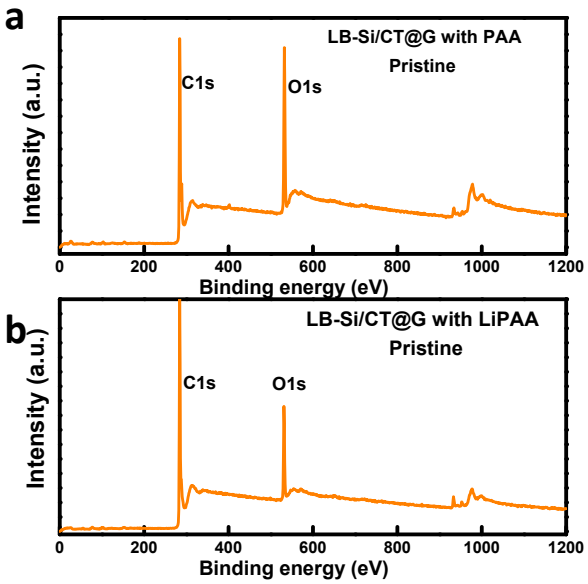

Figure S13. XPS analysis of LB-Si/CT@G with (a) PAA and (b) LiPAA before cycling.

Table S1 The material design and electrochemical properties of typical silicon-based anodes

Typical silicon anodes	Synthesis strategies	Main precursors	Synthesis conditions	Areal capacity	ICE	Ref.
Stress-Relieved Silicon Nanowires	Hydrothermal Treatment	Zinc Acetate; Germanium Oxide; Si foil	180 °C for 20 h	0.64 mAh cm^{-2}	60.4%	[1]
Hierarchical Graphene-Scaffolded Silicon/Graphite Composites	Ball milling and acid assisted self-assembly	Silicon; Graphite; Graphene oxide; Ascorbic acid	700 °C for 2 h; Ar/H_2	0.62 mAh cm^{-2}	75.6%	[2]
Microstructure Controlled Porous Silicon Particles	Arc melting	Si, Al, Cu, and Fe metal	Electric arc furnace; >3000 °C	1.18 mAh cm^{-2}	80.3%	[3]
Silicon Nanoparticles Embedded in Micro-Carbon Sphere Framework	Hydrothermal Treatment	Si nanoparticles; Sucrose; Oxalic acid	200 °C for 10 h	1.4 mAh cm^{-2}	75%	[4]
1D silicon-based nanostructures with different internal spaces	Electrospinning	Polyvinylpyrrolidone; Tetraethyl orthosilicate; Acetic Acid	10 μL min^{-1} extrusion rate; 15 kV accelerating voltage	1.8 mAh cm^{-2}	77%	[5]
Colloidal Synthesized Silicon–Carbon Composite	Soft-template route	$C_{12}H_{25}$-Si; CTAB; Resorcinol; Formaldehyde	800 °C for 3 h; Ar	1.8 mAh cm^{-2}	43%	[6]
Nanoporous Silicon from Commercial Alloy	Vacuum distillation	Mg_2Si	900 °C; 10 Pa or lower	2.7 mAh cm^{-2}	85%	[7]
Silicon Anode Enhanced by “Sticky” Mucin-Inspired DNA-Polysaccharide Binder	Electrophoresis	Si nano powder; Alginate; Deoxyribonucleic acid	100 V for 25 min	2.4 mAh cm^{-2}	84.6%	[8]
Silicon Particle Anode Fabricated by Scalable Mechanical Pressing	Dry press	Tetraethoxysilane; Si nanoparticles; Resorcinol; Formaldehyde	17.6 MPa to 123 MPa	3.5 mAh cm^{-2}	76.9	[9]
Silicon-nanolayer-embedded Graphite anode	Chemical vapor deposition	Spherical graphite; Silane gas; High-purity acetylene	900 °C for 8 min	3.3 mAh cm^{-2}	92%	[10]

Silicon anode with all-carbon graphdiyne in-situ weaved	Cu catalyzed graphdiyne	Hexakis[(trimethylsilyl)ethynyl] benzene; Cu nanowire	Liquid-phase catalysis for 48 h	4.9 mAh cm^{-2}	67%	[11]
Amorphous TiO2 layer cooperated Si nanoparticle	Sol-gel approach	Titanium isopropylate; Si nanoparticle; Resorcinol; -Formaldehyde	700 °C for 3 h; N_2	1.1 mAh cm^{-2}	86.1%	[12]
Porous silicon anode with CVD induced carbon infilling	Thermal decomposition	SiO powder; Acetylene	950 °C for 5h; Ar	3.5 mAh cm^{-2}	77%	[13]
KGM/Si@SiO2 electrode	Liquid oxidation	Sulfuric acid; Hydrogen peroxide; Si nanoparticles	80 °C for 2h	1.6 mAh cm^{-2}	78.1%	[14]
amorphous silicon nanolayer/activated graphite anode	Chemical vapor deposition	Graphite; Nickel chloride; Ethane; Silane	1000 °C for 3 h; H_2	3.5 mAh cm^{-2}	93.8%	[15]
LB-Si/CT@G	Low-temperature boron modification; Ball milling;	Bulk Si; Carbon nanotube; Graphite	525 °C for 5 h; Ar	7.4 mAh cm^{-2}	88%	This work

Reference

[1] Ting He, Jianrui Feng, Yan Zhang, et al., Stress-Relieved Nanowires by Silicon Substitution for High-Capacity and Stable Lithium Storage, Adv. Energy Mater. 8 (2018) 1702805.

[2] Shanshan Zhu, Jianbin Zhou, Yong Guan, et al., Hierarchical Graphene-Scaffolded Silicon/Graphite Composites as High Performance Anodes for Lithium-Ion Batteries, Small 14 (2018) 1802457.

[3] Myungbeom Sohn, Dong Geun Lee, Hyeong-Il Park, et al., Microstructure Controlled Porous Silicon Particles as a High Capacity Lithium Storage Material via Dual Step Pore Engineering, Adv. Funct. Mater. 28 (2018) 1800855.

[4] Min-Gi Jeong, Hoang Long Du, Mobinul Islam, et al., Self-rearrangement of silicon nanoparticles embedded in micron carbon sphere framework for high-energy and long-life lithium-ion batteries, Nano Lett. 17 (2017) 5600-5606.

[5] Yoonkook Son, Soojin Sim, Hyunsoo Ma, et al., Exploring Critical Factors Affecting Strain Distribution in 1D Silicon-Based Nanostructures for Lithium-Ion Battery Anodes, Adv. Mater. 30 (2018) 1705430.

[6] Haiping Su, Alejandro A. Barragan, Linxiao Geng, et al., Colloidal Synthesis of Silicon@Carbon Composite Materials for Lithium-Ion Batteries, Angew. Chem. Int. Edit. 56 (2017) 10780-10785.

[7] Yongling An, Huifang Fei, Guifang Zeng, et al., Green, Scalable and Controllable Fabrication of Nanoporous Silicon from Commercial Alloy Precursor for High–Energy Lithium–Ion Batteries, ACS Nano 12 (2018) 4993-5002.

[8] Sunjin Kim, You Kyeong Jeong, Younseon Wang, et al., A “Sticky” Mucin-Inspired DNA-Polysaccharide Binder for Silicon and Silicon–Graphite Blended Anodes in Lithium-Ion Batteries, Adv. Mater. 30 (2018)

1707594.

[9] Dingchang Lin, Zhenda Lu, Po-Chun Hsu, et al., High Tap Density Secondary Silicon Particle Anodes by Scalable Mechanical Pressing for Lithium-ion Batteries, Energy Environ. Sci. 8 (2015) 2371-2376.

[10] Minseong Ko, Sujong Chae, Jiyoung Ma, et al., Scalable synthesis of silicon-nanolayer-embedded graphite for high-energy lithium-ion batteries, Nature Energy 1 (2016) 16113.

[11] Hong Shang, Zicheng Zuo, Le Yu, et al., Low-Temperature Growth of All-Carbon Graphdiyne on a Silicon Anode for High-Performance Lithium-Ion Batteries, Adv. Mater. 2018, 30, 1801459.

[12] Jianping Yang, Yunxiao Wang, Wei Li, et al., Amorphous TiO_2 Shells: A Vital Elastic Buffering Layer on Silicon Nanoparticles for High-Performance and Safe Lithium Storage, Adv. Mater. 2017, 29, 1700523.

[13] Ran Yi , Fang Dai , Mikhail L. Gordin, et al., Micro-sized Si-C Composite with Interconnected Nanoscale Building Blocks as High-Performance Anodes for Practical Application in Lithium-Ion Batteries, Adv. Energy Mater. 2013, 3, 295–300.

[14] Songtao Guo, Heng Li, Yaqian Li, et al., SiO_2-Enhanced Structural Stability and Strong Adhesion with a New Binder of Konjac Glucomannan Enables Stable Cycling of Silicon Anodes for Lithium-Ion Batteries, Adv. Energy Mater. 2018, 8, 1800434.

[15] Namhyung Kim, Sujong Chae, Jiyoung Ma, et al., Fast-charging high-energy lithium-ion batteries via implantation of amorphous silicon nanolayer in edge-plane activated graphite anodes, Nature Comm. 8(2017) 812.